https://doi.org/10.5194/egusphere-2025-4229
Preprint. Discussion started: 2 December 2025

Meteorological Evaluation of the MERRA-2 Reanalysis Dataset: Insights for the Indian Subcontinent

Chakradhar Reddy Malasani[1,2], Basudev Swain[3*], Ankit Patel[1,2], Arundathi Chandrasekharan[4], Aishwarya Singh[5], Nidhi L. Anchan[6], Rui Song[7], Amit Sharma[8], and Sachin S. Gunthe[1,2*]

[1]Centre for Atmospheric and Climate Sciences, Indian Institute of Technology Madras, Chennai, India
[2]Environmental Engineering Division, Department of Civil Engineering, Indian Institute of Technology Madras, Chennai, India
[3]Atmospheric, Oceanic and Planetary Physics, University of Oxford, U.K
[4]Climate System Research Unit, Finnish Meteorological Institute, Finland
[5]Max Planck Institute for Chemistry, Biogeochemistry Department, Mainz, Germany
[6]Department of Energy, Environmental, and Chemical Engineering, Washington University in Saint Louis, Missouri, USA
[7]National Centre for Earth Observation, Atmospheric, Oceanic and Planetary Physics, University of Oxford, Oxford, OX1 3PU, UK
[8]Department of Civil and Infrastructure Engineering, Indian Institute of Technology Jodhpur, Jodhpur, India

Correspondence: Basudev Swain (basudev.swain@physics.ox.ac.uk), Sachin S. Gunthe (s.gunthe@iitm.ac.in)

Abstract. MERRA-2 meteorological data is widely utilized across the Indian region to investigate various climatological phenomena, necessitating a thorough evaluation of its accuracy. This study evaluates the performance of MERRA-2 meteorological fields over the Indian region by combining radiosonde measurements with satellite observations from AIRS and TRMM, along with reanalysis data from NCEP/NCAR. Our analysis concentrated on important meteorological variables, such as temperature, precipitation, water vapor, wind components and tropopause pressure, examining them in multiple seasons and pressure levels. MERRA-2 demonstrates comparable seasonal and spatial variations in temperature relative to AIRS observations, with strong correlations ($r^2 > 0.85$) and root mean square errors (RMSE) ranging from $0.9\,\mathrm{K}$ to $2.5\,\mathrm{K}$ near the surface, decreasing to approximately $1\,\mathrm{K}$ at higher altitudes. However, MERRA-2 exhibits a cold bias closer to the surface and warm biases in the upper troposphere. Water vapor profiles reveal a wet bias, particularly in the lower to mid-troposphere, with RMSE increasing with altitude, from less than $20\,\%$ at $1000\,\mathrm{hPa}$ to more than $75\,\%$ at $300\,\mathrm{hPa}$. Significant discrepancies are found in zonal wind estimates in the lower troposphere, especially over the Tibetan region, where MERRA-2 overestimates wind speeds. Below $700\,\mathrm{hPa}$, Zonal winds show mean biases (MB) from -0.7 to $1.5\,\mathrm{ms^{-1}}$ and RMSEs between $0\,\mathrm{ms^{-1}}$ and $2.2\,\mathrm{ms^{-1}}$. Agreement improves above $700\,\mathrm{hPa}$, with MBs ranging from -0.5 to $0.6\,\mathrm{ms^{-1}}$, and zonal wind estimates outperform meridional winds (RMSE: $0\,\mathrm{ms^{-1}}$–$4.4\,\mathrm{ms^{-1}}$). MERRA-2 reasonably captures the spatial distribution and intensity of precipitation but overestimates rainfall over complex terrain during the summer monsoon by up to $20\,\mathrm{mm\,d^{-1}}$ compared to TRMM data. Tropopause pressure comparisons show good agreement with AIRS (MB: -2 to $3\,\mathrm{hPa}$; RMSE: $2\,\mathrm{hPa}$–$4\,\mathrm{hPa}$), though larger biases are evident against radiosonde data (MB: $11\,\mathrm{hPa}$–$29\,\mathrm{hPa}$). These findings underscore the robustness of MERRA-2 in representing regional meteorological variability over the Indian region, while also highlighting specific biases, particularly in the lower troposphere and over complex terrain—that require careful consideration. As MERRA-2 data are frequently used as input for climate and chemical transport models, identifying and quantifying these biases is essential for improving model

https://doi.org/10.5194/egusphere-2025-4229
Preprint. Discussion started: 2 December 2025

accuracy and enhancing the reliability of atmospheric simulations. This study offers critical insights for developing more robust modeling frameworks.

1 Introduction

The Indian subcontinent features a diverse and complex geographical landscape, extending from the western Hindu Kush mountain ranges to the Arakan Mountains in the east, and from the towering Himalayas in the north to the expansive Indian Ocean in the south. This unique topographic variation drives substantial spatiotemporal variability in meteorological features and climatic zones. These variations play a pivotal role in shaping major weather phenomena such as the Indian monsoon, cyclonic activities, and extreme weather events like heatwaves and droughts, all of which are strongly influenced by the prevailing meteorological conditions (Mahto et al., 2023; Bajrang et al., 2023; Rai and Raveh-Rubin, 2023; Shahi and Rai, 2023; Kathayat et al., 2021). These climatic impacts, in turn, exert significant socio-economic effects, particularly in agriculture, a key pillar of the Indian economy, which is highly sensitive to regional meteorological variability (Datta et al., 2022; Aggarwal, 2003). Irregular rainfall patterns, frequent droughts, and flooding lead to fluctuations in crop yields, with direct implications for food security and economic stability (Datta et al., 2022; Aggarwal, 2003; Sharma et al., 2022).

To monitor regional meteorological parameters, numerous observational sites and field campaigns have been established across India. These efforts, while differing in spatial and temporal coverage, have yielded valuable datasets for understanding regional climate behavior. Notable campaigns include PACIFIC (2016–2018) (Lombard et al., 2023), ICARB (2006–2015) (Moorthy et al., 2008), WiFEX (2016–2017) (Ghude et al., 2017), CAIPEEX (2009–2012) (Kulkarni et al., 2009), and ACAM (active since 2015) (Tanimoto et al., 2020). Despite advancements in ground-based and satellite-based observational systems, limitations persist, particularly over remote and topographically complex areas due to high maintenance costs and incomplete spatial and temporal coverage. These gaps hinder comprehensive monitoring and accurate long-term assessment of regional meteorological trends.

While in-situ observations offer critical insights under a variety of environmental conditions, they also underscore the need for complementary datasets to fill coverage gaps. In this context, reanalysis datasets have emerged as essential tools for studying regional climate variability across India. Reanalyses provide continuous, gridded meteorological fields that enhance the spatial and temporal coherence lacking in observational networks. This approach provides a more consistent understanding of meteorological influences across both land and oceanic regions. Among the available datasets, the Modern-Era Retrospective Analysis for Research and Applications, Version 2 (MERRA-2) stands out as particularly valuable. (Gelaro et al., 2017), developed by NASA, has become one of the most widely used datasets. MERRA-2 assimilates a lot of observational data sources to provide high-resolution meteorological fields (Gelaro et al., 2017).

Beyond meteorological analysis, MERRA-2 plays a vital role as input for numerous climate models and chemical transport models (CTMs) (Anchan et al., 2024; Malasani et al., 2024; Swain et al., 2024). These offline CTMs rely on accurate, high-resolution meteorological fields for initialization and boundary conditions to simulate atmospheric composition and understand climate variability (Anchan et al., 2024; Malasani et al., 2024; Swain et al., 2024). While both regional and global

https://doi.org/10.5194/egusphere-2025-4229
Preprint. Discussion started: 2 December 2025

climate models (GCMs) are valuable tools, their reliability hinges on the quality of the input meteorological data. Fine-scale regional processes, such as land-sea interactions and topographic complexity, are often poorly resolved in global models, which underscores the importance of providing accurate meteorological inputs. MERRA-2 is frequently used for this purpose due to its global coverage and temporal continuity. However, despite its widespread use (Wen et al., 2022; Lacima et al., 2022; Wargan et al., 2017), MERRA-2 has not been comprehensively evaluated over the Indian region, particularly in terms of its ability to capture regional meteorological variability and associated biases (Wang et al., 2004; Zhao and Li, 2015; Seinfeld et al., 2016).

Moreover, MERRA-2 data is being used in providing meteorological input or boundary conditions for both regional and global CTMs focused on simulating atmospheric composition over India and other parts of the world (Anchan et al., 2024; Malasani et al., 2024; Swain et al., 2024). Given this widespread application, it is imperative to evaluate the accuracy, consistency and reliability of MERRA-2 over the Indian subcontinent to ensure robust climate and air quality simulations.

While advances in bias correction and data assimilation have significantly reduced uncertainties in reanalysis products (Dee et al., 2011; Gelaro et al., 2017), a thorough quantification of these uncertainties remains necessary to enhance the applicability of such datasets in weather forecasting, climate research, and chemical transport modeling. The study seeks to analyze the performance and applicability of MERRA-2 in representing spatio-temporal meteorological conditions over the Indian subcontinent by identifying and quantifying its biases. This evaluation provides critical insights into regional climate variability and supports the improvement of future model simulations, ultimately contributing to more accurate predictions of extreme meteorological events.

2 Datasets and evaluation methodology

2.1 MERRA-2 Data

This study investigates meteorological fields derived from MERRA-2 (Gelaro et al., 2017), which include wind components, temperature, specific humidity, surface pressure, and precipitation. NASA's Global Modeling and Assimilation Office (GMAO) at the Goddard Space Flight Center produces the offline assimilated meteorological products from which these datasets are obtained. MERRA-2 provides a high-resolution global dataset, represented on a horizontal grid of 0.5° latitude × 0.625° longitude, with 72 vertical pressure levels extending from the surface up to 0.01 hPa The dataset features a temporal resolution of 1 hour for surface-level mixing depth variables and 3 hours for other atmospheric variables. As the most recent reanalysis product developed by GMAO, MERRA-2 represents significant advancements over its predecessor, MERRA, with improvements in both the underlying general circulation model and the observational data assimilation system (Wen et al., 2022).

https://doi.org/10.5194/egusphere-2025-4229
Preprint. Discussion started: 2 December 2025

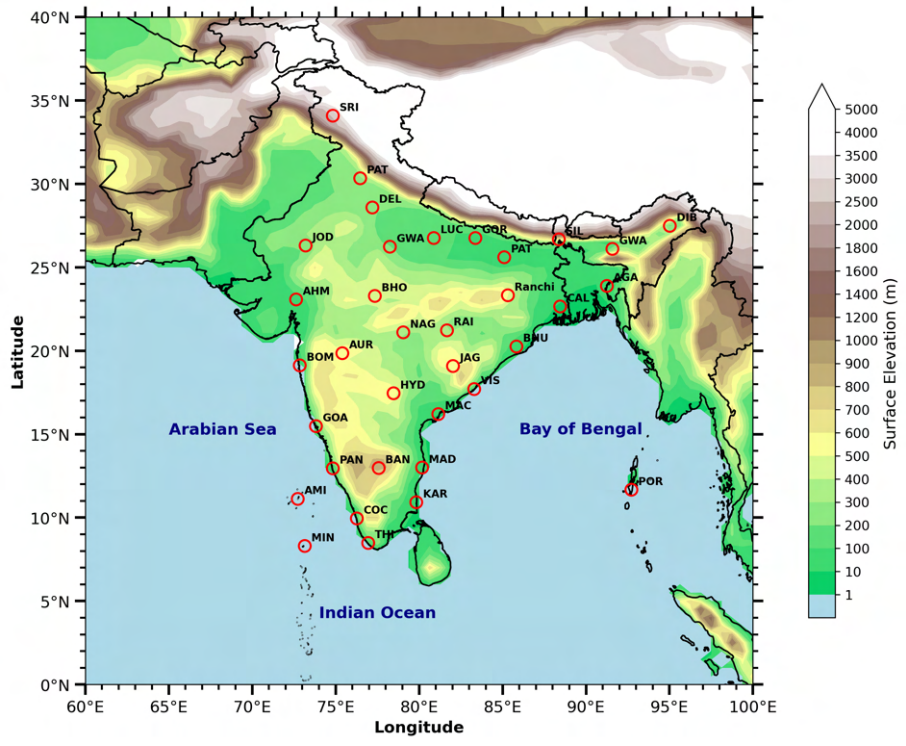

Figure 1. The study area and its topographical features are illustrated, along with the geographic positions of the radiosonde (RAOB) stations utilised for this analysis. Station codes corresponding to each site are detailed in Table 6.

The improved observational framework in MERRA-2 integrates measurements from advanced satellite sensors, including the Infrared Atmospheric Sounding Interferometer (IASI) and the Advanced Technology Microwave Sounder (ATMS), leading to better accuracy and representation of key meteorological parameters (McCarty et al., 2016).

MERRA-2 products have been extensively used in a wide range of atmospheric chemistry and air quality studies across South Asia, demonstrating their ability to reasonably capture spatiotemporal patterns of chemical evolution (Kara and Elbir; Wen et al., 2022; Hamal et al., 2020). The reliability of these applications is fundamentally linked to the accuracy of the meteorological fields.

The present work evaluates how well MERRA-2 meteorological data represent conditions over the Indian subcontinent (as shown in Fig. 1) by comparing it against multiple independent datasets, including radiosonde observations (RAOB), satellite retrievals from AIRS and TRMM, and reanalysis data from NCEP/NCAR. The analysis involves a detailed quantification of biases across these observational platforms to assess the consistency and reliability of MERRA-2 in capturing regional meteorological conditions.

https://doi.org/10.5194/egusphere-2025-4229
Preprint. Discussion started: 2 December 2025

2.2 Radiosonde Observations

Radiosonde measurements of tropopasue pressure, dew point temperature and temperature were obtained from the Integrated Global Radiosonde Archive (IGRA) https://www.ncei.noaa.gov/data/integrated-global-radiosonde-archive/. Data from 35 stations across the Indian region were utilised, and the stations were classified into four regions based on geographical features: island, coastal, low-altitude (0–500 m), and moderately high-altitude (500–1000 m). Further details provided in Fig. 1 and Table 6.

The radiosonde data are reported at twelve standard pressure levels: (100; 150, 200, 250, 300, 400, 500, 600, 700, 850, 925 and 1000) hPa. Observations are made globally at synchronized times—0000 UTC and 1200 UTC daily—and undergo rigorous quality control procedures to ensure data reliability (Walker, 2014; Durre et al., 2006). Radiosonde data have been widely utilized for satellite retrieval validation and atmospheric model evaluations (Iturbide-Sanchez et al., 2014; Fujiwara et al., 2025; Alghamdi, 2020).

2.3 Satellite-Borne Observations

Remote sensing provides an efficient approach for continuous monitoring of atmospheric conditions. In this study, satellite-based observations from two major platforms- Tropical Rainfall Measuring Mission (TRMM) and Atmospheric Infrared Sounder (AIRS). AIRS is a hyperspectral infrared sounder aboard NASA's Aqua satellite, consisting of 2378 infrared channels and 4 visible/near-infrared channels. With a swath width of 1652 km, AIRS achieves a horizontal resolution of 13.5 km and vertical resolution near 1 km, enabling precise retrievals of temperature, humidity, and cloud properties. It measures Earth's outgoing radiation across wavelengths of 0.4–1.0 μm and 3.7–15.4 μm (Divakarla et al., 2006b). For this study, temperature and water vapor retrievals from AIRS v5-Lev2 standard products were utilized, which have been previously validated using various in-situ and airborne observations. More information is available at https://airs.jpl.nasa.gov/mission/overview/ and https://aqua.nasa.gov/content/airs.

For precipitation analysis, we employed Version 7 of the TRMM 3B42 dataset, derived from the Tropical Rainfall Measuring Mission, a collaborative effort between NASA and the Japan Aerospace Exploration Agency (JAXA) which was launched in Nov. 1997 to monitor rainfall in tropical and subtropical regions and to assess the associated latent heating. TRMM provides 3-hourly precipitation estimates at a spatial resolution of 0.25° × 0.25°, covering the region from 50°S to 50°N and 180°W to 180°E (Gautam and Pandey, 2022; Shukla and Shukla, 2020; Kesarwani et al., 2023). The 3B42 is integrated product multi-satellite observations which provides a reliable rainfall estimates, particularly over the Indian region. Data can be accessed at https://pmm.nasa.gov/data-access/downloads/trmm.

2.4 Reanalysis Dataset

he MERRA-2 wind fields, including the zonal (U) and meridional (V) components, were further compared with the corresponding fields from the NCEP/NCAR reanalysis. Developed jointly by NOAA and NCAR, this long-term global dataset

https://doi.org/10.5194/egusphere-2025-4229
Preprint. Discussion started: 2 December 2025

incorporates historical observations from weather stations, satellites, and buoys through advanced data assimilation techniques (Kalnay et al., 1996). It provides a consistent, high-resolution depiction of global atmospheric fields.

Reanalysis product of NCEP/NCAR is available at 2.5° × 2.5° spatial resolution over global grids (144 longitudinal × 73 latitudinal points), spanning 0°E–357.5°E and 90°S–90°N. It spans 17 pressure levels (1000–10 hPa) and 28 sigma levels. Data are available four times daily (0Z, 6Z, 12Z, and 18Z) via https://psl.noaa.gov. This reanalysis product has been widely employed in meteorological and climate studies over the Indian region (Mojgan et al., 2017; Rai and Dimri, 2017).

2.5 Evaluation Methodology

For the spatio-temporal evaluation of MERRA-2 meteorology against various ground-based and satellite-borne observations, the year 2010 was chosen due to its meteorological stability (Mujumdar et al., 2012; Xavier et al., 2010). Mujumdar et al. (2012) analyzed the 2010 Asian summer monsoon within the context of La Niña conditions, finding that the monsoon's behavior closely aligned with climatological averages. This confirms 2010 as a representative and relatively stable year for climatological studies (Mujumdar et al., 2012).

The evaluation involves comparisons of MERRA-2 atmospheric fields with measurements from radiosonde observations, satellite retrievals (AIRS and TRMM), and the NCEP/NCAR reanalysis dataset. Both temporal and spatial analyses were conducted for all key meteorological parameters, including temperature, water vapor, wind components, and precipitation.

For spatial matching, each station was mapped to its corresponding MERRA-2 grid point using the nearest grid index (i, j) within the reanalysis domain. We applied bilinear interpolation based on the values of the four surrounding grid points to estimate the MERRA-2 values at the station location. For temporal comparisons, MERRA-2 outputs were averaged over time windows corresponding to the observational time stamps (0000 UTC and 1200 UTC), ensuring consistency across datasets.

Quality control procedures were followed to ensure the reliability of AIRS satellite retrievals. In accordance with the AIRS Science Team guidelines, only retrievals flagged with the highest quality assurance—typically associated with clear-sky conditions—were used in this study (Divakarla et al., 2006b). These quality flags also help identify unreliable retrievals, particularly at higher altitudes, leading to variability in the number of accepted profiles across different pressure levels.

For water vapor retrievals, additional filtering was applied based on the methodology described by Olsen et al. (2005), discarding profiles with negative values or errors exceeding 50%. Both water vapor and temperature are provided as layer-averaged valuesfrom AIRS . For consistency, the MERRA-2 profiles were derived by averaging values across two successive AIRS pressure levels., thus enabling direct layer-by-layer comparison. All evaluations were carried out on both spatial and temporal scales to provide a comprehensive assessment of MERRA-2 performance across the Indian subcontinent.

2.6 Statistical Metrics

To evaluate the accuracy of MERRA-2 against observations, several statistical measures were applied, including Mean Bias (MB), Root Mean Square Error (RMSE), and its systematic and random components ($RMSE_s$ and $RMSE_u$), Coefficient of Determination (r^2) and the Index of Agreement (IOA) (Willmott, 1981).

https://doi.org/10.5194/egusphere-2025-4229
Preprint. Discussion started: 2 December 2025

he Mean Bias (MB) quantifies the average tendency of a model to overestimate or underestimate a parameter and is defined as:

$$MB = \frac{1}{N}\sum_{i=1}^{N}(O_i - M_i) \tag{1}$$

where O_i is the i-th observed value, M_i is the corresponding value from MERRA-2, and N is the number of total paired observations.

The strength of the linear relationship between MERRA-2 and observation is measured by the (r^2), which is the square of Pearson's corr. coefficient (r):

$$r = \frac{\sum_{i=1}^{N}(O_i - \overline{O})(M_i - \overline{M})}{\sqrt{\sum_{i=1}^{N}(O_i - \overline{O})^2 \sum_{i=1}^{N}(M_i - \overline{M})^2}} \tag{2}$$

Above, $\overline{O}$ and $\overline{M}$ represent the mean of observations and modeled values, respectively.

The IOA (d) quantifies the degree of model-observation agreement, ranging from 0 (no agreement) to 1 (perfect agreement), and is computed as:

$$d = 1 - \frac{N \cdot RMSE^2}{\sum_{i=1}^{N}\left(|O_i - \overline{O}| + |M_i - \overline{O}|\right)^2} \tag{3}$$

The RMSE measures the average magnitude of the error without regard to its direction:

$$RMSE = \sqrt{\frac{1}{N}\sum_{i=1}^{N}(O_i - M_i)^2} \tag{4}$$

While RMSE quantifies the overall error magnitude, it does not distinguish between systematic (bias-related) and unsystematic (random) errors. Therefore, RMSE is decomposed into systematic RMSE ($RMSE_s$) and unsystematic RMSE ($RMSE_u$) components, which together satisfy:

$$RMSE^2 = RMSE_s^2 + RMSE_u^2 \tag{5}$$

And Unsystematic RMSE is:

$$RMSE_u = \sqrt{(1 - r^2)\sigma_M^2} \tag{6}$$

where σ_M^2 is the variance of the MERRA-2 dataset. Once $RMSE_u$ is determined, $RMSE_s$ can be found using Equation 5.

https://doi.org/10.5194/egusphere-2025-4229
Preprint. Discussion started: 2 December 2025

3 Results

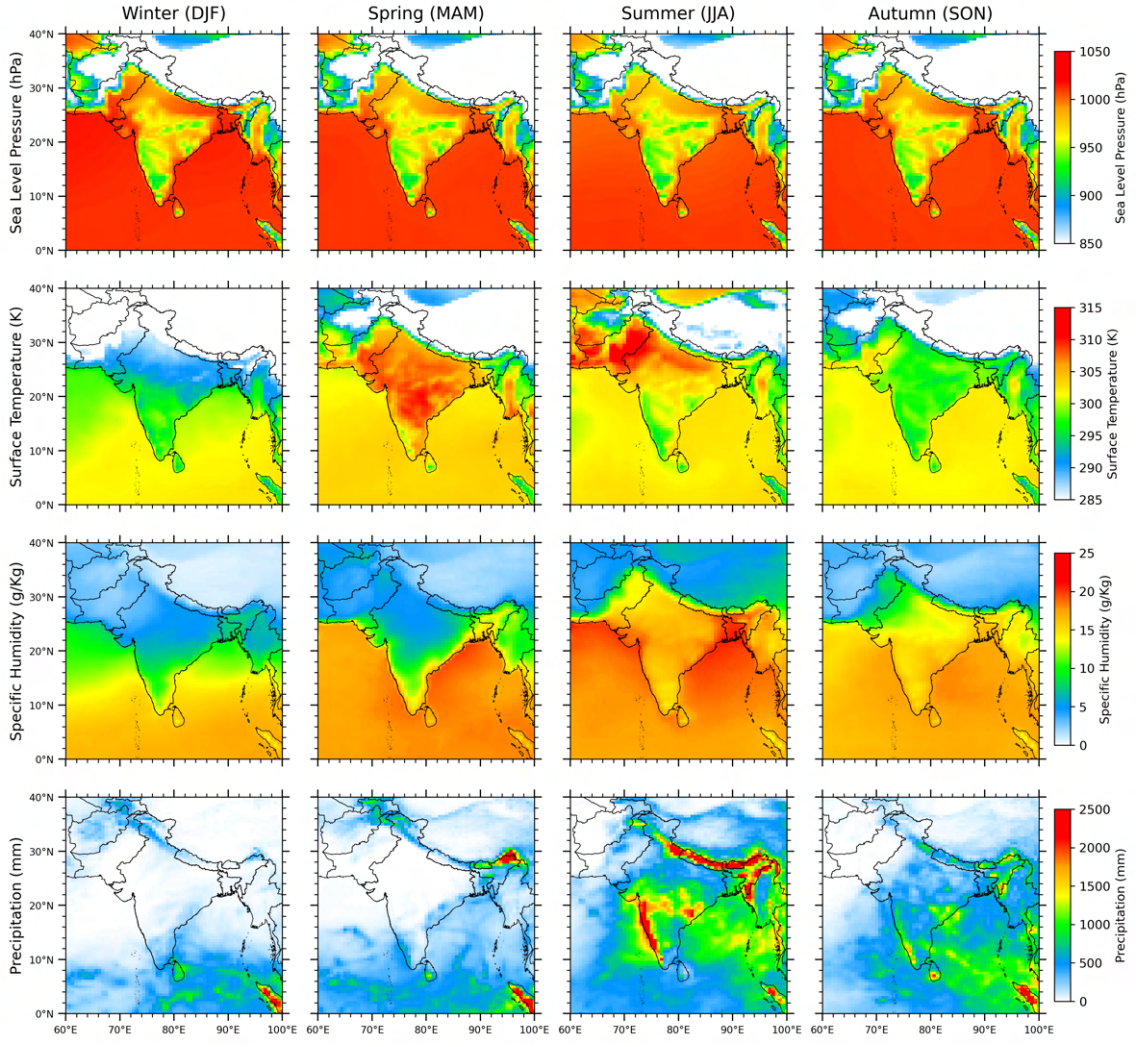

Figure 2. Spatial distribution of seasonally averaged surface pressure (hPa), specific humidity ($g\,kg^{-1}$), surface temperature (K) and total precipitation (mm) from MERRA-2 for all the four seasons respectively.

The spatial distribution of seasonally averaged surface pressure (hPa), specific humidity ($g\ kg^{-1}$), surface temperature (K) and precipitation (mm) derived from MERRA-2 for the each season of 2010—winter (DJF), spring (MAM), summer (JJA), and autumn (SON) is shown in Fig. 2. Seasonal variations in surface pressure across different regions of India are generally minimal. However, compared to summer, regions north of 20°N experience somewhat larger variations, around 5 hPa. Notably, the southern Indian peninsula, especially along the western coast, exhibits smaller differences of approximately 2 hPa. Other variables display pronounced seasonal cycles, with extreme values typically occurring in summer or winter. Spatial variations

https://doi.org/10.5194/egusphere-2025-4229
Preprint. Discussion started: 2 December 2025

in surface temperature are most prominent during winter and summer, while temperature distributions are relatively uniform during spring and autumn. In summer, higher surface temperatures are observed over the northwestern desert regions, with a north-south gradient of 15–20°C; this gradient decreases to about 5–8°C during winter. Regional differences in temperature magnitude across seasons reflect variations in solar heating over diverse landscapes and the influence of regional meteorological factors (Kumar et al., 2012). This gradient strongly influences weather patterns and monsoon circulation, ultimately shaping the timing and intensity of the Indian summer monsoon ((Weldeab et al., 2022)). In contrast, the Kerala region experiences slightly higher temperatures (about 1°C) in winter compared to summer. During spring, surface temperatures are roughly 5°C higher over central India and the southern peninsula. Surface pressure remains relatively constant in the Bay of Bengal and Arabian Sea, showing little seasonal variation. Similarly, surface temperature and specific humidity over these oceanic regions remain stable throughout spring, summer, and autumn. In contrast, precipitation exhibits clear seasonal variability across both continental and oceanic areas. During winter and spring, most continental regions have specific humidity below 10 g/kg, increasing to over 14 g/kg during summer and autumn. Summer precipitation peaks over the Himalayan foothills, eastern India, central India, and the Western Ghats, often exceeding 2000 mm across the landmass. Autumn precipitation decreases to 400-600 mm with notable spatial variability, while winter and spring are characterized by minimal precipitation.

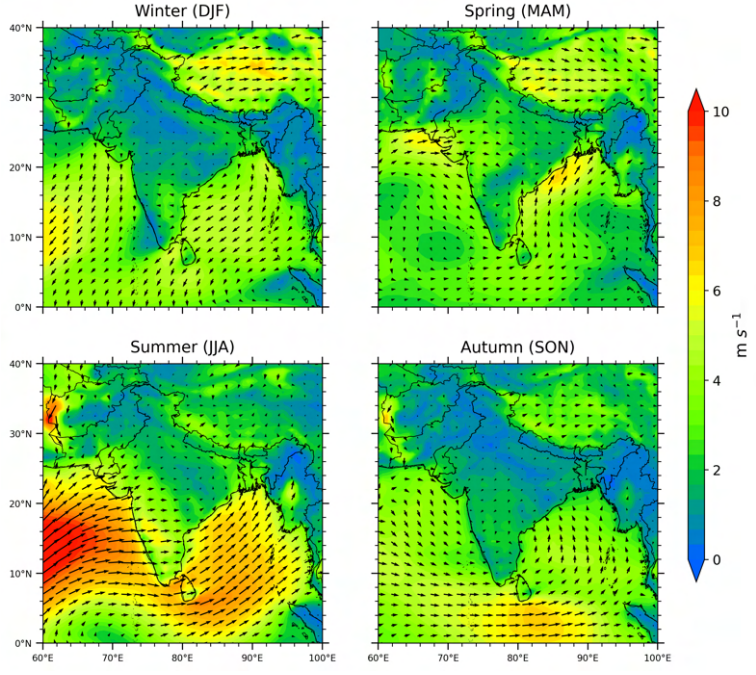

Figure 3. Seasonal average wind vectors and wind speeds ($m\,s^{-1}$) derived from MERRA-2 over the study area for all four seasons of 2010.

The average wind speeds and vectors from MERRA-2 for all four seasons are shown in Fig. 3. The patterns suggest that, regardless of season, continental surface winds are generally weaker than marine winds, likely due to greater surface roughness over land (Kumar et al., 2012). Winds are stronger in summer than winter, as Ekman drift associated with the southwest

https://doi.org/10.5194/egusphere-2025-4229
Preprint. Discussion started: 2 December 2025

monsoon intensifies surface flow, contributing to substantial sea-salt aerosol production in the Arabian Sea (Satheesh et al., 2010).

During northern winters, continental air is colder and denser than oceanic air, reflected in higher surface pressure over land (Fig. 2). Consequently, low-level northerly or northeasterly winds flow from the continent toward the equator driven by this pressure gradient (Sijikumar et al., 2016). Wind vectors over the Himalayan region and Tibetan Plateau during winter are typically southwesterly (Zhu et al., 2024). In early spring, rapid heating of the continental region (Fig. 2) establishes a low-pressure and high-pressure system over land and oceans repsectively. This pressure contrast drives near-surface westerly winds over northern India, northward winds over the Arabian Sea, and southerly winds over the Bay of Bengal. As spring progresses, continued warming creates favorable conditions for the South Asian monsoon onset in early summer, which is marked by the establishment of prevailing southwesterly winds. As summer transitions to autumn, cooling of the landmass causes winds to shift toward the northeast. Summer exhibits the strongest winds among all seasons, facilitating the transport of moisture-laden air from the oceans inland, which corresponds with the highest specific humidity and precipitation values seen in Fig. 2.

The South Asian climate follows a distinct seasonal cycle characterized by changes in temperature, humidity, rainfall, and wind patterns. The MERRA-2 dataset effectively captures these variations. In the following sections, we evaluate its accuracy by comparing it against satellite observations, reanalysis datasets, and radiosonde measurements. This comprehensive assessment will help determine the reliability of MERRA-2 for use in climate modeling as initial and boundary condition data.

https://doi.org/10.5194/egusphere-2025-4229
Preprint. Discussion started: 2 December 2025

3.1 AIRS Temperature and Water Vapor

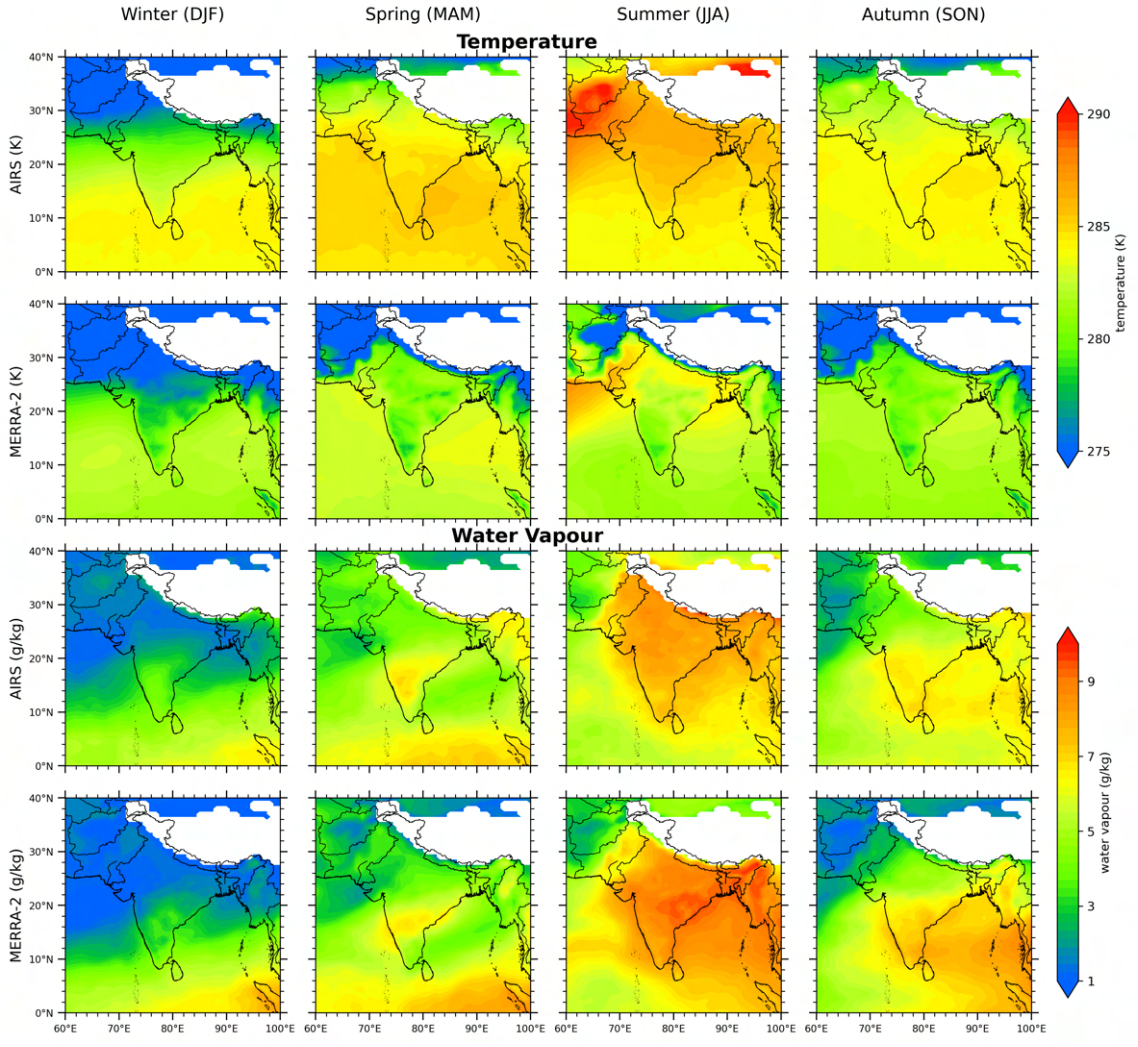

Figure 4. Seasonal spatial distributions of atmospheric temperature (rows 1-2) and water vapor (rows 3-4) at 700 hPa, derived from co-located AIRS and MERRA-2 data for 2010 for each of the four seasons: winter (DJF), spring (MAM), summer (JJA), and autumn (SON). White areas denote missing data.

A comparison between temperature (K) and water vapor (g kg^{-1}) retrieved from AIRS and MERRA-2 is shown in Fig. 4. As mentioned in Section 2.5, all data points are co-located spatially and temporally before quality control. The spatial distribution of both AIRS and MERRA-2 shows in increase in the magnitudes of temperatures and water vapor at 700 hPa from winter to summer, followed by a decrease. A strong north-south gradient of temperatures is there in MERRA-2 than the AIRS tem-

https://doi.org/10.5194/egusphere-2025-4229
Preprint. Discussion started: 2 December 2025

peratures over the Indian subcontinent. In each season, discrepancies between AIRS and MERRA-2 temperature are evident, especially in summer. These differences are more dominant above 20°N.

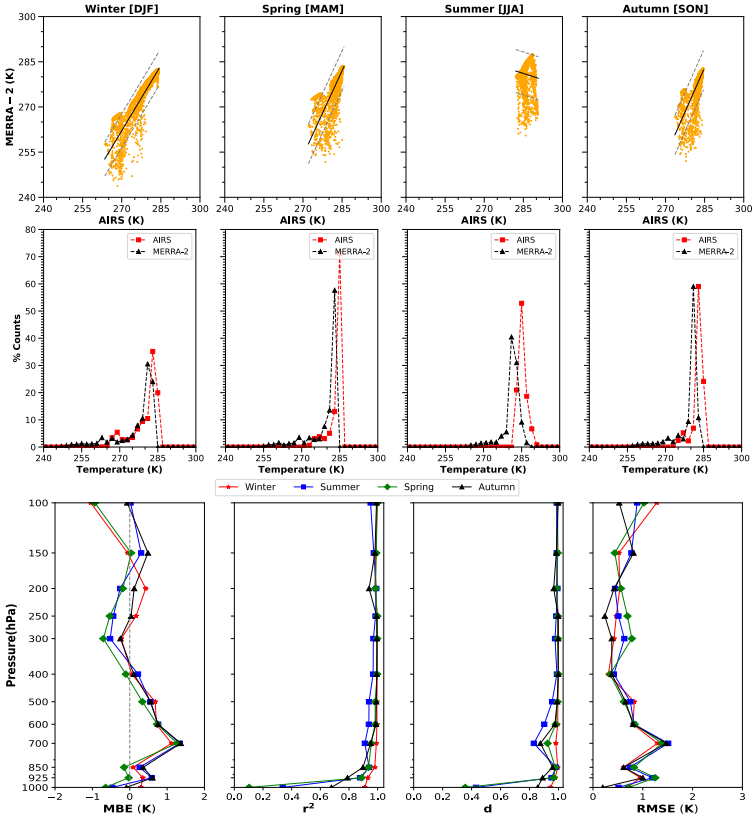

Figure 5. A comparison of AIRS and MERRA-2 temperature (k) at 700 hPa for the year 2010. The top panel displays scatter plots of the data for each of the four seasons, with black lines representing the linear fit and grey shading indicates the 95% confidence intervals. The middle panel shows the corresponding frequency analyses, binned at 2 k intervals. The bottom panel provides vertical profiles for each season, detailing key statistical metrics: *MB,* r^2 *, d, RMSE*

Fig. 5 focuses on the statistical evidence of the relationship between AIRS and MERRA-2 datasets. There is a strong correla-
225 tion between AIRS and MERRA-2 temperatures in all seasons. This relationship shows good agreement at every pressure level from 1000 to 100 hPa, with temperature values being very close at each level. Frequency analysis also indicates a common peak between both datasets at 280–284 K across all seasons. The $r^2 > 0.85$ for all seasons except summer, particularly below 850 to 925 hPa. These temperature differences are further analysed through vertical profiles from 1000 to 100 hPa using r^2, IOA (d), RMSE, and MB, as shown in Fig. 5. The vertical profile of MB between AIRS and MERRA-2 temperatures lies
230 within ∼1 K throughout all pressure levels. Just above the surface, MERRA-2 temperature is slightly cold-biased, and this cold bias decreases around 400 hPa. MERRA-2 temperature is warm-biased at 400–200 hPa and 150–100 hPa levels; otherwise, it

https://doi.org/10.5194/egusphere-2025-4229
Preprint. Discussion started: 2 December 2025

remains cold-biased throughout the vertical profile. The degree of agreement and r^2 remain very high (> 0.90) at all levels for each season. The RMSE in temperature near the surface is 0.2–0.7 K and approximately ∼1 K at other pressure levels.

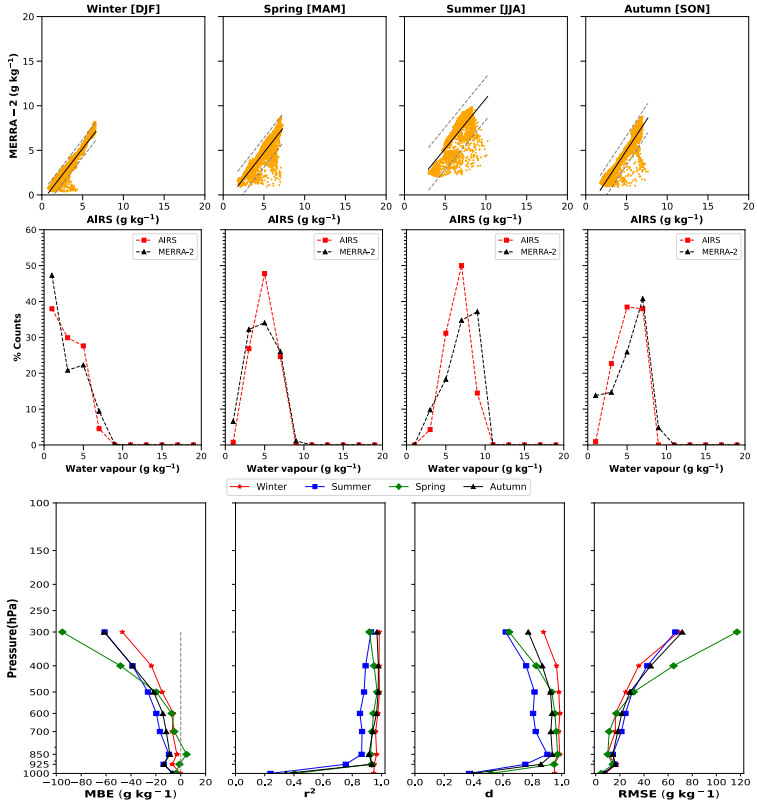

Figure 6. specific humidity (g/kg) comparison between AIRS and MERRA-2 at 700 hPa. Top panel is contains scatter plots of these datasets in each season, with black lines representing the linear fit and grey shading indicates the 95% confidence intervals. The middle panel shows the corresponding frequency analyses. The below shows vertical profiles in each season, detailing key statistical metrics: *MB,* r^2 *, d, RMSE*

Similarly, AIRS water vapor is found to be in good agreement with simulated water vapor in all seasons. AIRS and MERRA-2 water vapor differ within 5% of the averaged value. Vertical levels from 1000 to 300 hPa exhibit good agreement between AIRS and MERRA-2 water vapor, as presented in Table 3.1. Given the limited sensitivity of AIRS to upper-tropospheric water vapor, the statistical evaluations in this study were restricted to levels up to 300 hPa. (Divakarla et al., 2006a). There is good correlation in all seasons except summer, possibly due to large spatial variability in water vapor caused by the southwest monsoon. The scatter plot in Fig. 6 shows a stronger correlation in winter compared to other seasons.

Similar to the temperature comparison, Fig. 6 also displays vertical profiles of*MB,* r^2 *, d, RMSE*. Except for summer, where the values are lower but still show significant correlation, the r^2 values are quite high. At all pressure levels, from 1000 to 300 hPa, results are consistently biased toward wetter conditions compared to AIRS retrievals. RMSE increases significantly with altitude; this rise at higher altitudes may be due to inaccuracies in temperature simulation and reduced AIRS sensitivity

https://doi.org/10.5194/egusphere-2025-4229
Preprint. Discussion started: 2 December 2025

Table 1. Seasonal mean vertical temperature profiles from MERRA-2 and AIRS datasets.

Pressure (hPa)	Winter		Spring		Summer		Autumn	
	MERRA-2*	AIRS*	MERRA-2*	AIRS*	MERRA-2*	AIRS*	MERRA-2*	AIRS*
1000	298.3 ± 1.7	298.6 ± 1.3	300.8 ± 0.3	300.2 ± 0.2	300.4 ± 0.3	299.9 ± 0.2	299.6 ± 0.3	299.6 ± 0.2
925	292.2 ± 3.0	292.6 ± 3.3	298.0 ± 3.7	298.0 ± 3.2	296.7 ± 2.9	297.3 ± 2.6	294.8 ± 1.7	295.4 ± 1.3
850	288.0 ± 4.3	288.1 ± 4.2	293.9 ± 3.0	293.8 ± 2.6	293.5 ± 2.8	293.8 ± 2.8	291.0 ± 1.6	291.3 ± 1.5
700	279.3 ± 4.4	280.5 ± 4.9	282.5 ± 2.3	283.7 ± 2.5	283.9 ± 1.9	285.2 ± 1.5	281.6 ± 1.7	283.0 ± 2.1
600	272.2 ± 5.3	272.9 ± 5.4	274.6 ± 3.0	275.4 ± 3.0	276.8 ± 1.3	277.6 ± 1.2	274.7 ± 2.5	275.4 ± 2.5
500	262.7 ± 6.2	263.4 ± 6.3	265.9 ± 3.7	266.2 ± 3.9	269.3 ± 1.9	269.9 ± 1.6	266.5 ± 3.3	267.0 ± 3.4
400	251.5 ± 7.0	251.5 ± 7.0	254.7 ± 4.5	254.6 ± 4.7	259.4 ± 2.0	259.6 ± 2.0	255.9 ± 4.0	256.0 ± 4.1
300	236.7 ± 7.0	236.5 ± 6.8	240.0 ± 5.3	239.3 ± 5.1	245.6 ± 2.0	245.1 ± 2.0	241.6 ± 3.8	241.3 ± 3.8
250	227.7 ± 5.9	227.9 ± 5.5	230.5 ± 5.0	230.0 ± 4.6	235.9 ± 2.1	235.5 ± 2.0	232.1 ± 2.7	232.1 ± 2.6
200	218.4 ± 2.3	218.8 ± 2.2	220.2 ± 2.6	220.0 ± 2.2	223.6 ± 2.7	223.4 ± 2.5	220.9 ± 1.3	221.0 ± 1.0
150	208.8 ± 3.5	208.7 ± 3.2	209.4 ± 3.2	209.4 ± 2.9	208.9 ± 3.7	209.2 ± 3.3	207.6 ± 3.5	208.1 ± 3.1
100	198.9 ± 6.7	197.8 ± 7.4	198.5 ± 6.5	197.6 ± 6.8	196.4 ± 4.0	196.5 ± 3.8	196.6 ± 5.3	196.5 ± 5.0

* $Mean \pm 1Sigma$

Table 2. AIRS water vapor (g kg^{-1}); same as teh analysis presented in Table 3.1.

Pressure (hPa)	Winter		Spring		Summer		Autumn	
	MERRA-2*	AIRS*	MERRA-2*	AIRS*	MERRA-2*	AIRS*	MERRA-2*	AIRS*
1000	14.4 ± 3.1	14.3 ± 2.1	18.0 ± 0.4	17.3 ± 0.5	17.8 ± 0.3	16.8 ± 0.4	17.1 ± 0.5	16.0 ± 0.4
925	10.4 ± 4.4	9.7 ± 3.1	11.7 ± 4.3	11.5 ± 3.0	15.6 ± 2.2	13.7 ± 1.7	13.8 ± 2.9	12.1 ± 2.1
850	6.7 ± 2.9	6.5 ± 2.6	8.0 ± 2.7	8.4 ± 2.4	11.5 ± 2.7	10.5 ± 2.0	9.7 ± 2.8	8.9 ± 2.2
700	3.3 ± 1.9	3.1 ± 1.6	5.2 ± 1.6	4.9 ± 1.3	7.6 ± 1.9	6.5 ± 1.2	5.8 ± 2.0	5.2 ± 1.4
600	2.1 ± 1.6	2.0 ± 1.4	3.3 ± 1.4	3.1 ± 1.0	5.8 ± 1.6	4.9 ± 1.0	4.1 ± 1.8	3.6 ± 1.3
500	1.2 ± 1.1	1.1 ± 0.9	1.9 ± 1.1	1.6 ± 0.8	4.1 ± 1.2	3.3 ± 0.9	2.6 ± 1.2	2.1 ± 0.9
400	0.6 ± 0.5	0.5 ± 0.4	1.0 ± 0.7	0.7 ± 0.4	2.2 ± 0.7	1.6 ± 0.5	1.3 ± 0.7	1.0 ± 0.5
300	0.2 ± 0.2	0.2 ± 0.1	0.4 ± 0.2	0.2 ± 0.1	0.7 ± 0.2	0.5 ± 0.1	0.4 ± 0.2	0.3 ± 0.1

* $Mean \pm 1Sigma$

caused by decreasing water vapor mixing ratios with altitude. RMSE values for AIRS versus MERRA-2 water vapor profiles are under 20% , rising rapidly to over 75% at 300 hPa. The MERRA-2 wet bias may lead to overestimation of hydroxyl radical concentrations, which could cause underestimation of various volatile organic compounds, thus affecting ozone concentrations. According to the evaluation, these indicators fall within suggested criteria. When MERRA-2 serves as boundary conditions,

https://doi.org/10.5194/egusphere-2025-4229
Preprint. Discussion started: 2 December 2025

errors in simulated water vapor are unlikely to significantly affect air quality modeling, provided other sources of error are absent.

3.2 Meridional and Zonal components of Winds-NCEP

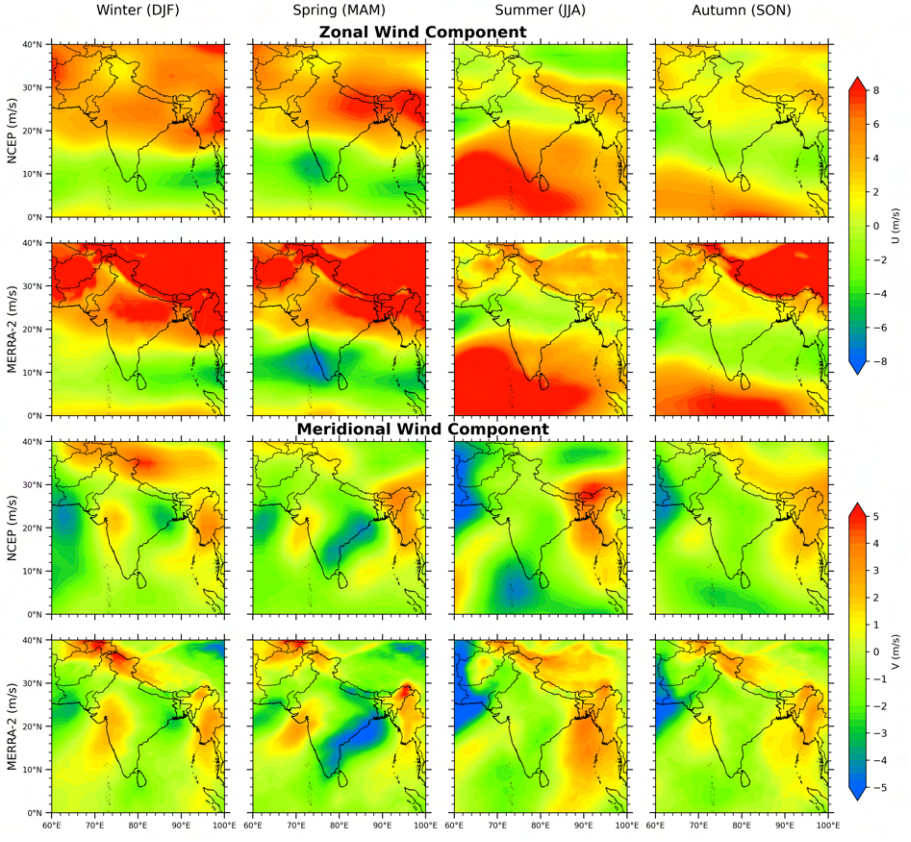

Figure 7. Spatial distributions of seasonally averaged zonal (top two panels) and meridional wind fields (bottom two panels) at 700 hPa, derived from co-located NCEP and MERRA-2 datasets for each season of 2010. White areas denote missing data.

Figure 7 presents the spatial distribution of seasonally averaged zonal and meridional wind fields at 700 hPa for 2010, of MERRA-2 and NCEP reanalysis datasets. The spatial patterns of meridional wind components from both NCEP and MERRA-2 exhibit a high degree of similarity. However, MERRA-2 overestimates zonal wind over the Tibetan region in all seasons except summer, where both datasets show similar values. Wind values from MERRA-2 align well with corresponding NCEP values at pressure levels from 700 to 100 hPa, but differences are observed between 1000 and 700 hPa (Tables 3 and 4). The meridional wind component exhibits larger discrepancies compared to the zonal component. Correlation between datasets improves with altitude.

https://doi.org/10.5194/egusphere-2025-4229
Preprint. Discussion started: 2 December 2025

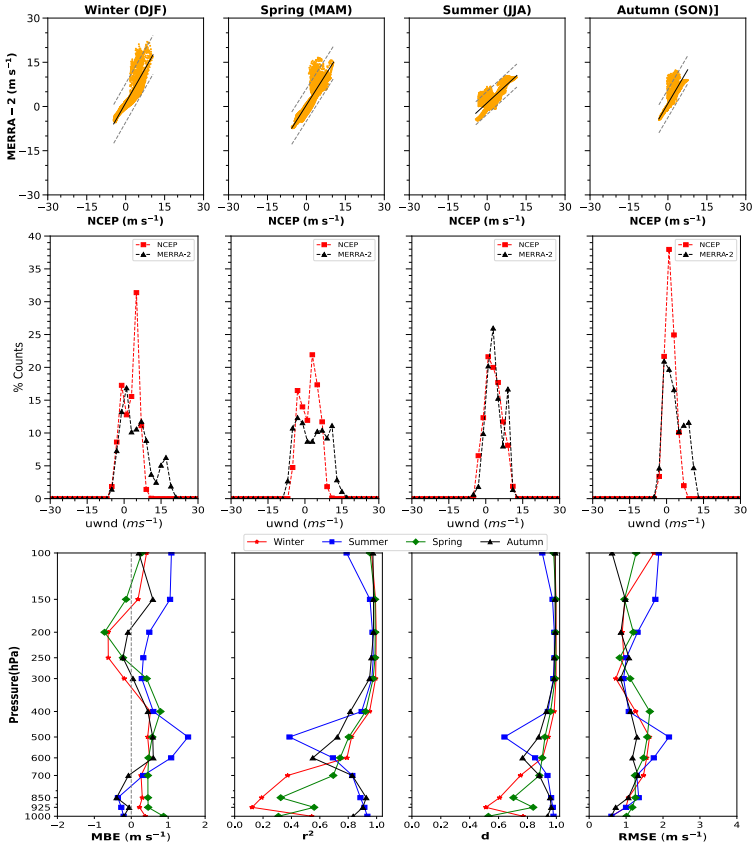

Figure 8. NCEP and MERRA-2 comparison of zonal wind components at 700 hPa. Above panel shows scatter plots of each seasons, with black lines representing the linear fit and the grey shading indicates the 95% confidence intervals. The middle panel shows the corresponding frequency analyses. Below panel is vertical profiles of each season, detailing key statistical metrics: *MB, r^2, d, RMSE.*

Figs. 8 and 9 present vertical profiles of statistical analysis for each season. Although significant differences exist in wind components at lower levels, correlation improves between 700 and 100 hPa. These differences may not be apparent in scatter plots (Figs. 8 and 9), which show reasonable positive correlations, but the vertical profiles highlight poorer correlation at lower levels. Frequency analyses for both datasets show similar distributions for zonal and meridional winds.

https://doi.org/10.5194/egusphere-2025-4229
Preprint. Discussion started: 2 December 2025

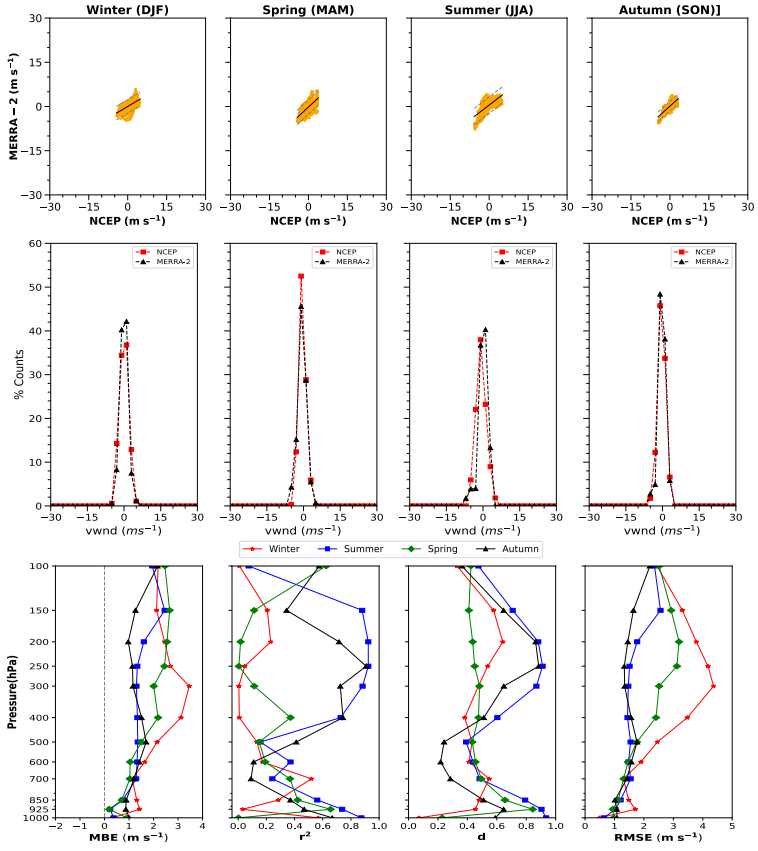

Figure 9. NCEP and MERRA-2 comparison of meridional wind components at 700 hPa. Above panel shows scatter plots of each seasons, with black lines representing the linear fit and the grey shading indicates the 95% confidence intervals. The middle panel shows the corresponding frequency analyses. Following panel shows vertical profiles in each season, detailing key statistical metrics: *MB, r^2, d, RMSE.*

Among all seasons, summer shows the best correlation for both wind components. MB, r^2, d, and RMSE improve above 600 hPa for both components. The r^2 and (d) for meridional wind across all pressure levels are lower compared to zonal wind, with best values between 600–100 hPa: zonal $r^2 : 0.75\tilde{}0.99$, $d : 0.86\tilde{}0.99$; meridional $r^2 : 0.65\tilde{}0.99$, $d : 0.80\tilde{}0.99$. MB and RMSE are lower for zonal wind (-0.7–1.5 m s^{-1} and 0.6–2.2 m s^{-1}) than meridional wind (0.2–3.4 m s^{-1} and 0.5–4.4 m s^{-1}) at lower levels (1000–700 hPa), with errors decreasing with altitude. Summer exhibits the most improved values. Overall, systematic discrepancies appear at lower levels for both components, while upper levels (600–100 hPa) show similar behavior between datasets.

The wind speed evaluation criteria of Emery et al. (2001) were adopted, which recommend MB values within ± 0.5 m s^{-1}, an index of agreement of $d > 0.6$,and RMSE below 2 m s^{-1}. For both wind components, MB, d, and RMSE generally satisfy these thresholds between 1000 and 100 hPa, with the exception of the meridional wind at higher pressure levels during winter and spring.

https://doi.org/10.5194/egusphere-2025-4229
Preprint. Discussion started: 2 December 2025

Table 3. Mean and standard deviation of the seasonally averaged zonal wind component from NCEP and MERRA-2 across the domain. The data is shown across pressure levels from 1000 to 100 hPa, for the year 2010

Pressure (hPa)	Winter		Spring		Summer		Autumn	
	NCEP	MERRA-2	NCEP	MERRA-2	NCEP	MERRA-2	NCEP	MERRA-2
1000	1.68 ± 0.69	2.06 ± 0.56	2.14 ± 0.48	3.02 ± 0.58	5.75 ± 2.21	5.55 ± 2.09	5.04 ± 1.36	4.84 ± 1.10
925	2.02 ± 1.02	2.24 ± 0.51	3.36 ± 1.58	3.82 ± 1.41	7.02 ± 3.27	6.75 ± 3.17	5.72 ± 2.12	5.66 ± 1.74
850	2.28 ± 1.11	2.58 ± 0.70	3.38 ± 1.40	3.84 ± 0.98	7.33 ± 3.78	6.97 ± 3.35	5.83 ± 2.92	5.44 ± 2.22
700	5.24 ± 1.81	5.50 ± 1.32	4.79 ± 2.08	5.24 ± 1.61	5.95 ± 2.92	6.27 ± 2.36	4.54 ± 2.49	4.46 ± 1.44
600	8.62 ± 3.00	9.12 ± 2.13	7.01 ± 2.71	7.48 ± 2.08	4.45 ± 2.48	5.53 ± 2.05	4.26 ± 1.49	4.86 ± 0.95
500	13.26 ± 3.74	13.70 ± 3.30	9.60 ± 3.20	10.17 ± 2.48	3.72 ± 1.92	5.26 ± 1.40	6.27 ± 2.15	6.85 ± 1.59
400	19.49 ± 5.15	20.00 ± 5.00	12.99 ± 4.56	13.78 ± 3.70	7.84 ± 2.47	8.44 ± 1.95	12.24 ± 2.36	12.69 ± 1.98
300	27.70 ± 8.03	27.51 ± 8.17	18.21 ± 6.28	18.62 ± 5.89	14.51 ± 3.56	14.79 ± 2.89	20.80 ± 3.63	20.85 ± 3.29
250	32.39 ± 10.10	31.77 ± 9.95	22.47 ± 7.24	22.25 ± 7.02	17.99 ± 4.67	18.31 ± 3.99	25.79 ± 4.80	25.56 ± 4.20
200	36.39 ± 11.19	35.77 ± 11.04	26.88 ± 8.43	26.16 ± 7.94	20.55 ± 5.91	21.04 ± 5.14	29.39 ± 5.47	29.30 ± 5.12
150	35.49 ± 10.16	35.67 ± 10.42	27.36 ± 8.19	27.22 ± 7.77	19.45 ± 5.94	20.51 ± 5.11	27.93 ± 5.10	28.51 ± 5.27
100	26.17 ± 8.80	26.59 ± 8.27	20.22 ± 5.05	20.51 ± 4.34	11.60 ± 3.32	12.69 ± 2.75	18.85 ± 3.53	19.05 ± 3.62

* $mean \pm 1Sigma$

3.3 Precipitation-TRMM

The comparison of precipitation patterns derived from TRMM and MERRA-2 datasets, along with their differences (bottom panel), is illustrated in Fig. 10. Both data sets capture the spatial distribution of high rainfall in the western Ghats, the Himalayan foothills, and parts of eastern India. The annual mean precipitation over continental India is 1434.98 mm based on TRMM data and 1579.82 mm from MERRA-2, indicating a bias of approximately 10.1%. Both datasets consistently show a clear seasonal cycle, with maximum rainfall occurring during the summer (contributing 43.0% of annual precipitation in both TRMM and MERRA-2) and minimum during winter (12.0% in TRMM and 11.6% in MERRA-2). MERRA-2 successfully captures the seasonal variability evident in the TRMM observations.

https://doi.org/10.5194/egusphere-2025-4229
Preprint. Discussion started: 2 December 2025

Table 4. Mean and standard deviation of the seasonally averaged meridonal wind component from NCEP and MERRA-2 across the domain. The data is shown across pressure levels from 1000 to 100 hPa, for the year 2010.

Pressure (hPa)	Winter		Spring		Summer		Autumn	
	NCEP	MERRA-2	NCEP	MERRA-2	NCEP	MERRA-2	NCEP	MERRA-2
1000	0.97 ± 0.26	1.30 ± 0.12	0.68 ± 0.29	1.60 ± 0.21	3.18 ± 1.38	3.56 ± 1.13	1.77 ± 0.67	2.78 ± 0.60
925	1.02 ± 0.49	2.44 ± 0.90	2.70 ± 1.51	2.89 ± 0.96	3.76 ± 1.92	3.99 ± 1.47	1.94 ± 0.83	2.81 ± 0.77
850	1.11 ± 0.65	2.42 ± 0.76	1.64 ± 1.14	2.34 ± 0.67	2.84 ± 1.41	3.59 ± 1.21	1.59 ± 0.61	2.48 ± 0.44
700	1.70 ± 0.93	2.83 ± 0.62	1.77 ± 1.01	2.80 ± 0.51	1.85 ± 0.96	3.14 ± 0.64	1.46 ± 0.79	2.67 ± 0.33
600	1.59 ± 1.03	3.23 ± 0.63	1.65 ± 1.13	2.69 ± 0.56	1.64 ± 0.80	2.97 ± 0.54	1.21 ± 0.71	2.63 ± 0.27
500	1.49 ± 1.15	3.64 ± 0.95	1.58 ± 0.86	3.09 ± 0.78	1.65 ± 0.75	3.01 ± 0.57	1.16 ± 0.62	2.85 ± 0.31
400	1.71 ± 0.87	4.82 ± 1.35	1.49 ± 0.53	3.67 ± 1.25	1.69 ± 1.01	3.03 ± 0.86	1.40 ± 0.62	2.91 ± 0.78
300	2.85 ± 1.08	6.31 ± 2.52	2.05 ± 0.72	4.06 ± 1.60	2.35 ± 1.96	3.65 ± 1.92	1.84 ± 0.74	3.00 ± 1.19
250	5.32 ± 1.82	8.01 ± 3.06	3.20 ± 1.03	5.64 ± 1.71	3.13 ± 2.38	4.46 ± 2.53	3.46 ± 1.69	4.60 ± 2.07
200	6.60 ± 2.61	9.05 ± 3.00	4.39 ± 1.41	6.94 ± 1.50	3.94 ± 2.30	5.54 ± 2.60	5.27 ± 1.84	6.24 ± 2.01
150	5.77 ± 2.78	7.90 ± 1.80	3.59 ± 1.07	6.25 ± 1.06	3.70 ± 1.74	6.15 ± 2.06	4.86 ± 1.11	6.12 ± 1.19
100	2.43 ± 0.91	4.62 ± 0.71	1.55 ± 0.63	4.02 ± 0.85	2.08 ± 0.62	4.03 ± 1.36	1.80 ± 0.55	3.97 ± 0.60

$^* mean \pm 1 Sigma$

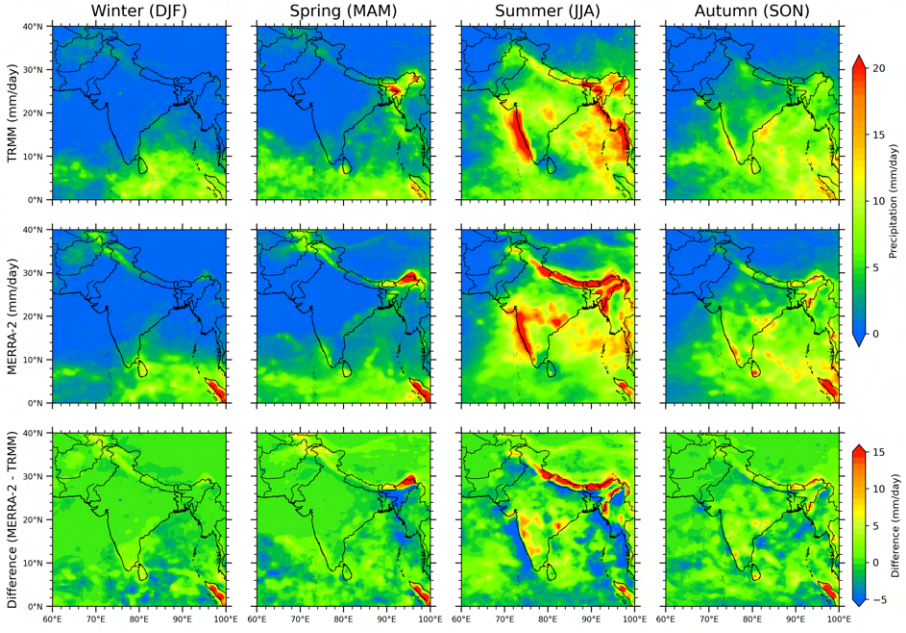

Figure 10. Spatially distributed total precipitation from co-located TRMM and MERRA-2 data for each season of 2010. The bottom row displays the corresponding seasonal differences in precipitation values between the two datasets.

https://doi.org/10.5194/egusphere-2025-4229
Preprint. Discussion started: 2 December 2025

The Himalayan regions and parts of eastern India receive higher precipitation in both summer and winter, influenced by western disturbances (Westerlies), which are represented in both datasets. This winter precipitation plays a crucial role in supporting rabi crops and sustaining glacier mass, which subsequently contributes to river flow during other seasons (YADAV et al., 2012). Additionally, higher rainfall is observed over southern India during the autumn season.

Quantitatively, MERRA-2 precipitation closely aligns with TRMM data, though the largest differences occur in summer, with biases ranging from approximately –5 to +15 mm/day across the subcontinent. MERRA-2 tends to show higher precipitation along the Himalayan foothills, sometimes exceeding 20 mm/day, levels that TRMM generally underestimates. Conversely, MERRA-2 underestimates rainfall in regions such as the Indo-Gangetic Plain near the Himalayan foothills and eastern India. These discrepancies may be attributed to TRMM inaccuracies over complex terrain, particularly along India's eastern and western coastal regions (Nair et al., 2009).

Previous studies have reported that both global and regional climate models encounter challenges in accurately simulating the South-Asian monsoon (Rajan and Desamsetti, 2021). These limitations are linked to the complex monsoon dynamics, diverse regional topography, and localized convection processes. Such conditions also contribute to reduced retrieval accuracy in TRMM during the summer monsoon, a period marked by strong spatial gradients in temperature and precipitation, prevalent warm cloud systems, and heterogeneous terrain (Indu and Nagesh Kumar, 2014; Shukla et al., 2019).

https://doi.org/10.5194/egusphere-2025-4229
Preprint. Discussion started: 2 December 2025

3.4 Radiosonde Observations – Temperature

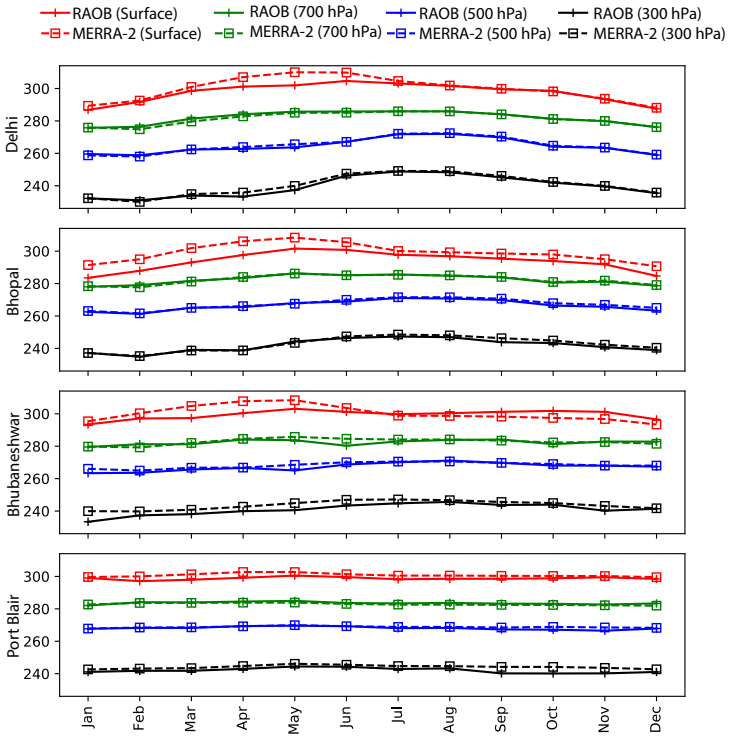

Figure 11. Seasonal changes in atmospheric temperature during 2010 are compared between co-located radiosonde observations and MERRA-2 data. The analysis covers four distinct locations: Delhi, Bhopal, Bhubaneshwar and Port Blair and the profiles are presented at the surface as well as at 700 500 and 300 hPa levels.

MERRA-2 temperature data are validated against radiosonde (RAOB) observations from 34 stations within the study area (Table 6, Fig. 1). Figure 11 illustrates the monthly temperature variations of four distinct locations: Delhi, Bhopal, Bhubaneshwar and Port Blair at the surface as well as at 700 500 and 300 hPa levels. Seasonal temperature variation is more pronounced at Delhi and Bhopal compared to Bhubaneshwar and Port Blair. Notable differences in surface temperature are observed between January and May at most sites, except at Port Blair. Overall, MERRA-2 temperatures show good agreement with radiosonde observations across all pressure levels and seasons.

https://doi.org/10.5194/egusphere-2025-4229
Preprint. Discussion started: 2 December 2025

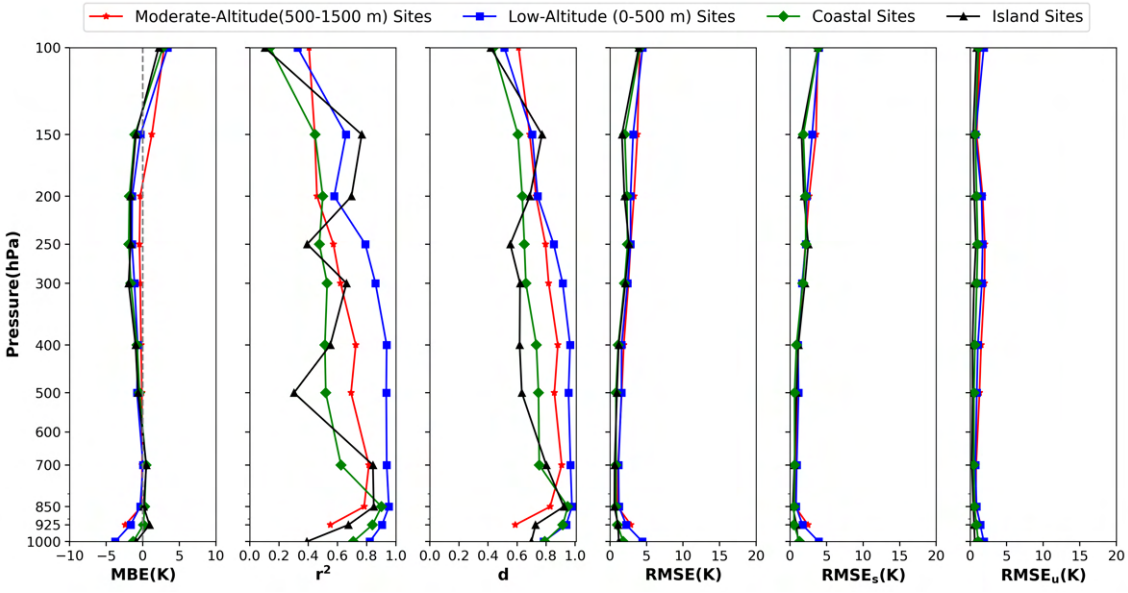

Figure 12. Vertical profiles of temperature statistics are compared across all four category sites.

Vertical profiles of temperature statistics for four category sites are illustrated in Figure 12. The correlation (r^2) coefficient is strong for low-altitude stations from 1000 to 250 hPa, peaking at 850 hPa and decreasing above. Moderately high-altitude stations show stronger r^2 above 700 hPa, while coastal and island stations exhibit weaker and more variable correlations. Mean Bias (MB) is more pronounced at low- and moderate-altitude stations below 850 hPa, ranging from 0 to 4 K below 300 hPa. RMSE and its components generally vary between 0 and 4 K, decreasing up to 850 hPa and increasing at higher levels. The reduced correlation at coastal and island sites is likely associated with inaccuracies in the model's surface representation at these locations. Furthermore, discrepancies between the actual elevation of the station and the topography assigned to the model (Table 6) can contribute to temperature biases in the reanalysis data.

3.5 Tropopause Pressure- Radiosonde and AIRS

Accurate assessment of tropopause pressure is essential as it signifies changes in atmospheric properties and affects the exchange of air and pollutants near tropopause. The tropopause plays a key role in regulating the budgets of trace gases like ozone and water vapor. In this study, tropopause pressure is calculated following threshold lapse-rate method given in (Reichler et al., 2003), since MERRA-2 does not provide it directly. We compare MERRA-2 tropopause pressure with AIRS retrievals and RAOB observations.

https://doi.org/10.5194/egusphere-2025-4229
Preprint. Discussion started: 2 December 2025

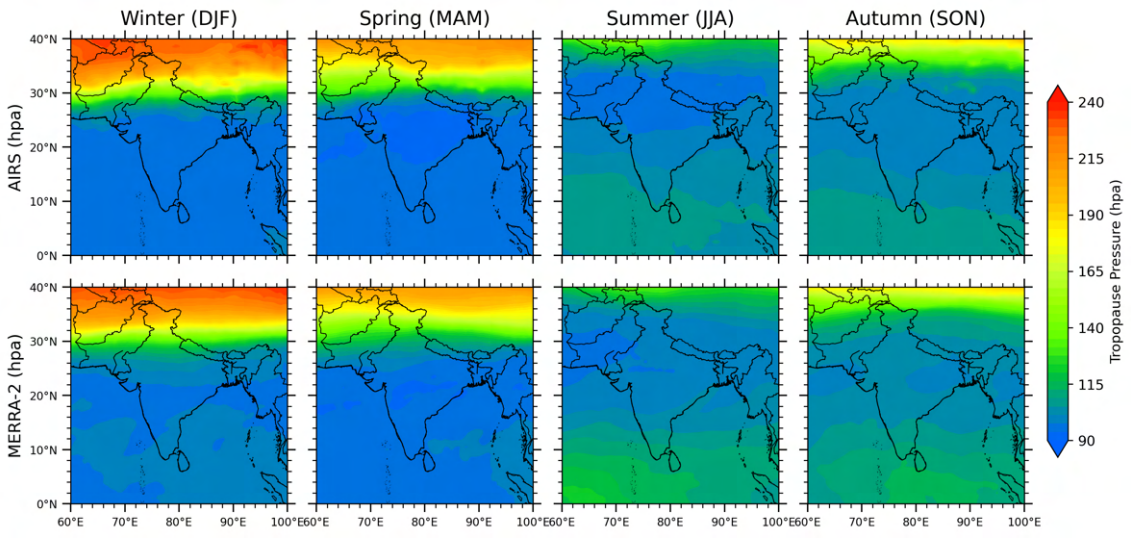

Figure 13. Spatial distribution of seasonal tropopause pressure, a co-located AIRS and MERRA-2 data during each season of 2010.

The seasonal spatial variation of tropopause pressure from AIRS and MERRA-2 is plotted in Fig. 13, showing similar spatial patterns across seasons. A pronounced north–south gradient in tropopause pressure is evident ((Meng et al., 2021)), particularly across 25°N latitude. The northern regions exhibit higher tropopause pressures, while the southern regions display lower values. MERRA-2 slightly overestimates tropopause pressure in the southern region (mean bias: 1.5 hPa) and slightly underestimates it in the northern region (mean bias: -2.06 hPa). Both datasets capture a clear seasonal cycle, with the lowest tropopause pressures during winter (125.35 hPa for AIRS and 124.79 hPa for MERRA-2) and the highest during summer (103.60 hPa for AIRS and 105.89 hPa for MERRA-2). The meridional gradient is weaker in summer and more pronounced in winter.The largest differences between AIRS and MERRA-2 over regions south of 25°N occur in summer (3.47 hPa), while the smallest occur in spring (0.94 hPa). Over regions north of 25°N, the greatest difference is observed in winter (-5.0 hPa), with negligible differences during autumn (-0.03 hPa). These latitudinal and seasonal variations likely reflect changes in solar radiation and atmospheric dynamics over subtropical latitudes.

Table 5. The table provides annual average and standard deviation of tropopause pressure from RAOB, AIRS, and MERRA-2. Mean bias (MB) and RMSE for the four site types are also listed, with values rounded to whole numbers.

Site Category	MERRA-2 vs RAOB Troposphere Pressure				MERRA-2 vs AIRS Troposphere Pressure			
	RAOB	MERRA-2	MB	RMSE	AIRS	MERRA-2	MB	RMSE
Low Altitude	157.38 ± 56.71	101.11 ± 4.04	-56.27	78.06	99.05 ± 4.89	101.0 ± 4.32	1.95	2.4
Moderately High	167.45 ± 72.59	105.66 ± 19.45	-61.79	87.47	104.96 ± 20.54	105.53 ± 17.98	0.57	2.43
Coastal	130.32 ± 27.57	101.32 ± 2.47	-29	39.67	98.81 ± 1.52	101.23 ± 2.26	2.41	2.55
Island	119 ± 4.90	99.96 ± 2.54	-19.04	19.94	100.36 ± 0.77	103.10 ± 0.76	2.74	2.76

https://doi.org/10.5194/egusphere-2025-4229
Preprint. Discussion started: 2 December 2025

Errors in MERRA-2 tropopause pressure were evaluated by comparison with RAOB and AIRS. Annual average values from RAOB and AIRS were compared with MERRA-2 for each site category (Table 5). Mean tropopause pressure values for MERRA-2 and AIRS were averaged from co-located data within a $0.5^\circ \times 0.625^\circ$ grid centered on each RAOB site. Yearly averages for MERRA-2 and AIRS are approximately 99–105 hPa, compared to RAOB values ranging 111–130 hPa. Mean bias (MB) and RMSE relative to RAOB are 11–29 hPa and 13–33 hPa, respectively; for AIRS, MB and RMSE range from -2 to 3 hPa and 2–4 hPa, respectively. The notable biases in MERRA-2 tropopause pressure are of concern for regions like the Himalayas, as an accurate representation of the tropopause is essential for correctly depicting stratosphere-troposphere exchange processes.

4 Summary and Discussions

This study provides a detailed evaluation of meteorological and atmospheric variables from the reanalysis dataset MERRA-2 over the Indian region.he MERRA-2 data are compared with observations from AIRS, NCEP reanalysis, TRMM precipitation data, and radiosonde observations. Objective was to examine the accuracy and consistency of these datasets across multiple atmospheric parameters, seasons, and vertical levels during the year 2010.

Temperature and water vapor comparison of AIRS with MERRA-2 highlights a generally strong agreement across all seasons and 1000 to 100 hPa pressure levels. Both datasets capture the expected seasonal variability, showing increases in temperature and moisture from winter to summer, followed by decreases thereafter. The spatial analysis reveals a pronounced north-south temperature gradient in MERRA-2 compared to AIRS, especially over the Indian subcontinent. Statistically, high correlation coefficients ($r^2 > 0.85$) and strong indices of agreement were found for temperature, except for some discrepancies below 850 hPa during summer, likely linked to local atmospheric dynamics. The mean bias in temperature remains within approximately 1 K throughout the vertical profile, with surface cold biases in MERRA-2 and warm biases at mid-tropospheric levels. Water vapor comparisons also show good agreement, with differences generally within 5% at levels below 300 hPa. However, higher altitudes reveal increasing discrepancies likely due to AIRS' reduced sensitivity and simulation uncertainties, with summer showing lower correlations attributed to monsoon-driven variability.

The evaluation of wind fields at 700 hPa from MERRA-2 and NCEP demonstrates similar spatial patterns, though MERRA-2 tends to overestimate zonal winds over the Tibetan Plateau except during summer. Correlations between the datasets improve with altitude, with better agreement observed above 600 hPa. The meridional wind component exhibits higher biases and errors at higher levels than the zonal component, reflecting systematic discrepancies. Nevertheless, the statistical benchmarks for wind speed proposed by (Emery et al., 2001) are met between 700 and 100 hPa, indicating acceptable performance of MERRA-2 for wind-driven transport modeling at these levels.

Precipitation comparisons using TRMM and MERRA-2 reveal that both datasets effectively capture the strong seasonal cycle of rainfall over India, with maximum precipitation during the summer monsoon. However, MERRA-2 tends to overestimate precipitation along the Himalayan foothills and shows spatial variability over complex terrain, likely reflecting limitations in

https://doi.org/10.5194/egusphere-2025-4229
Preprint. Discussion started: 2 December 2025

capturing fine-scale orographic effects. This highlights the ongoing challenge in accurately simulating monsoon rainfall due to complex topography and convective processes, and the inherent limitations of satellite retrievals in such regions.

Radiosonde temperature observations from 35 stations provide a valuable independent benchmark, confirming the general reliability of MERRA-2 temperature profiles across different altitudes and surface types. Correlations are strongest at lower altitudes and tend to weaken aloft, with biases remaining moderate. These results reinforce the consistency of MERRA-2 temperature simulations in representing vertical thermal structure over the Indian subcontinent.

Tropopause pressure derived from AIRS, MERRA-2, and radiosonde data exhibits consistent seasonal and latitudinal patterns, with lower spatial variability in summer and higher variability in winter. MERRA-2 tends to underestimate tropopause pressure compared to radiosondes, with biases up to 29 hPa, whereas AIRS shows better agreement with radiosonde data. Accurately representing the tropopause is crucial for modeling stratosphere-troposphere exchange, especially over the Himalayas where such processes impact regional air quality and trace gas budgets.

Overall, the evaluation underscores the robustness of MERRA-2 in simulating key meteorological fields and their seasonal cycles over India, with some systematic biases primarily occurring at lower atmospheric levels and over complex terrain. AIRS retrievals serve as a valuable observational complement, particularly for characterizing the upper troposphere and tropopause. The integration of these datasets with radiosonde and TRMM observations enhances confidence in the meteorological inputs used for regional climate and air quality modeling.

For future modeling efforts that intend to use MERRA-2 as a meteorological input, attention should be directed toward improving model parameterizations in the lower troposphere and refining representations of complex orographic regions to minimize biases. Additionally, incorporating higher-resolution observational datasets could help resolve fine-scale variability, particularly during the summer monsoon season when atmospheric conditions are highly dynamic and spatially heterogeneous.

https://doi.org/10.5194/egusphere-2025-4229
Preprint. Discussion started: 2 December 2025

Table 6. Description and classification of the Radiosonde observation sites employed in this study

Sr.No	Station Name	Station Code	Latitude (°N)	Longitude (°E)	Actual Altitude (m)	MERRA-2 Altitude (m)
Coastal sites						
1	Bhubaneswar	BHU	20.25	85.83	46	73
2	Bombay	BOM	19.12	72.85	14	97
3	Vishakapatnam	VIZ	17.70	83.30	66	35
4	Machilipatnam	MAC	16.20	81.15	3	2
5	Goa	GOA	15.48	73.82	60	76
6	Madras	MAD	13.00	80.18	16	49
7	Panambur	PAN	12.95	74.83	31	163
8	Karikal	KAR	10.92	79.83	7	3
9	Cochin	COC	9.95	76.27	3	47
10	Thiruvananthapuram	THI	8.48	76.95	64	86
Island sites						
11	Amini Divi	AMI	11.12	72.73	4	0
12	Port Blair	PBL	11.67	92.72	79	6
13	Minicoy	MIN	8.30	73.15	2	0
Low Altitude sites						
14	Patiala	PTA	30.33	76.47	251	257
15	Delhi	DEL	28.58	77.20	216	206
16	Dibrugarh	DIB	27.48	95.02	111	182
17	Jodhpur	JOD	26.30	73.20	224	258
18	Gwalior	GWA	26.23	78.25	207	256
19	Lucknow	LUC	26.75	80.88	128	128
20	Gorakhpur	GOR	26.75	83.30	77	81
21	Silguri	SIL	26.67	88.37	123	273
22	Gauhati	GAU	26.10	91.58	54	400
23	Patna	PTN	25.60	85.10	60	59
24	Agartala	AGA	23.88	91.25	16	25
25	Ahmedabad	AHM	23.07	72.63	55	47
26	Calcutta	KOL	22.65	88.45	6	5
27	Nagpur	NAG	21.10	79.05	310	337
28	Raipur	RAI	21.22	81.67	298	311
Moderately High Altitude sites						
29	Srinagar	SRI	34.08	74.83	1587	2632
30	Bhopal	BHO	23.28	77.35	523	475
31	Ranchi	RAN	23.32	85.32	652	426
32	Aurangabad	AUR	19.85	75.40	579	561
33	Jagdalpur	JAG	19.08	82.03	553	520
34	Hyderabad	HYD	17.45	78.47	545	495
35	Bangalore	BAN	12.97	77.58	921	842

https://doi.org/10.5194/egusphere-2025-4229
Preprint. Discussion started: 2 December 2025

Code availability. The code and data supporting the conclusions of this paper are available upon request.

Data availability. All the datasets used in this study are cited in the manuscript.

Acknowledgements. The authors thank Prof. Marco Vountas for his keen interest and valuable suggestions. NOAA provided both the Radiosonde data (http://www.esrl.noaa.gov/raobs/) and the NCEP/NCAR reanalysis datasets (http://www.esrl.noaa.gov/). The TRMM data were acquired from the Goddard Earth Sciences Data and Information Services Center (GES DISC) website (https://disc.gsfc.nasa.gov/datasets/TRMM_3B42_Daily_7/summary?keywords=TRMM_3B42_Daily_7). Ankit Patel acknowledges the financial support by DST-INSPIRE Fellowship, Project No. 2020/IF200113/SP23241491CE.

https://doi.org/10.5194/egusphere-2025-4229
Preprint. Discussion started: 2 December 2025

References

Aggarwal, P.: Impact of climate change on Indian agriculture, Journal of Plant Biology-new Delhi, 30, 189–198, 2003.

Alghamdi, A. S.: Evaluation of four reanalysis datasets against radiosonde over Southwest Asia, Atmosphere, 11, 402, 2020.

Anchan, N. L., Swain, B., Sharma, A., Singh, A., Malasani, C. R., Chandrasekharan, A., Kumar, U., Ojha, N., Liu, P., Vountas, M., et al.: Assessing the variability of Aerosol Optical Depth over India in response to future scenarios: Implications for carbonaceous aerosols, Journal of Geophysical Research: Atmospheres, 129, e2024JD040 846, 2024.

Bajrang, C., Attada, R., and Goswami, B.: Possible factors for the recent changes in frequency of central Indian Summer Monsoon precipitation extremes during 2005–2020, npj Climate and Atmospheric Science, 6, 120, 2023.

Datta, P., Behera, B., et al.: Climate change and Indian agriculture: A systematic review of farmers' perception, adaptation, and transformation, Environmental Challenges, 8, 100 543, 2022.

Dee, D. P., Uppala, S. M., Simmons, A. J., Berrisford, P., Poli, P., Kobayashi, S., Andrae, U., Balmaseda, M., Balsamo, G., Bauer, d. P., et al.: The ERA-Interim reanalysis: Configuration and performance of the data assimilation system, Quarterly Journal of the royal meteorological society, 137, 553–597, 2011.

Divakarla, M. G., Barnet, C. D., Goldberg, M. D., McMillin, L. M., Maddy, E., Wolf, W., Zhou, L., and Liu, X.: Validation of Atmospheric Infrared Sounder temperature and water vapor retrievals with matched radiosonde measurements and forecasts, Journal of Geophysical Research: Atmospheres, 111, 2006a.

Divakarla, M. G., Barnet, C. D., Goldberg, M. D., McMillin, L. M., Maddy, E., Wolf, W., Zhou, L., and Liu, X.: Validation of Atmospheric Infrared Sounder temperature and water vapor retrievals with matched radiosonde measurements and forecasts, Journal of Geophysical Research: Atmospheres, 111, 2006b.

Durre, I., Vose, R. S., and Wuertz, D. B.: Overview of the integrated global radiosonde archive, Journal of Climate, 19, 53–68, 2006.

Emery, C., Tai, E., and Yarwood, G.: Enhanced meteorological modeling and performance evaluation for two Texas ozone episodes, Prepared for the Texas natural resource conservation commission, by ENVIRON International Corporation, 161, 2001.

Fujiwara, M., Sun, B., Reale, A., Cimini, D., Larosa, S., Borg, L., von Rohden, C., Sommer, M., Dirksen, R., Maturilli, M., et al.: Justification for high ascent attainment for balloon radiosonde soundings at GRUAN and other sites, EGUsphere, 2025, 1–71, 2025.

Gautam, A. K. and Pandey, A.: Ground validation of GPM Day-1 IMERG and TMPA Version-7 products over different rainfall regimes in India, Theoretical and Applied Climatology, 149, 931–943, 2022.

Gelaro, R., McCarty, W., Suárez, M. J., Todling, R., Molod, A., Takacs, L., Randles, C. A., Darmenov, A., Bosilovich, M. G., Reichle, R., et al.: The modern-era retrospective analysis for research and applications, version 2 (MERRA-2), Journal of climate, 30, 5419–5454, 2017.

Ghude, S. D., Bhat, G., Prabhakaran, T., Jenamani, R., Chate, D., Safai, P., Karipot, A., Konwar, M., Pithani, P., Sinha, V., et al.: Winter fog experiment over the Indo-Gangetic plains of India, Current Science, pp. 767–784, 2017.

Hamal, K., Sharma, S., Khadka, N., Baniya, B., Ali, M., Shrestha, M. S., Xu, T., Shrestha, D., and Dawadi, B.: Evaluation of MERRA-2 precipitation products using gauge observation in Nepal, Hydrology, 7, 40, 2020.

Indu, J. and Nagesh Kumar, D.: Evaluation of TRMM precipitation products over Indian subcontinent, The International Archives of the Photogrammetry, Remote Sensing and Spatial Information Sciences, 40, 355–358, 2014.

https://doi.org/10.5194/egusphere-2025-4229
Preprint. Discussion started: 2 December 2025

Iturbide-Sanchez, F., Reale, A., Nalli, N. R., Divakarla, M., Gambacorta, A., Sun, B., Tan, C., Xiong, X., Maddy, E. S., and Wilson, M.: Enhanced validation of satellite derived sounding products using reference and dedicated radiosondes, in: 2014 United States National Committee of URSI National Radio Science Meeting (USNC-URSI NRSM), pp. 1–1, IEEE, 2014.

Kalnay, E., Kanamitsu, M., Kistler, R., Collins, W., Deaven, D., Gandin, L., Iredell, M., Saha, S., White, G., Woollen, J., Zhu, Y., Chelliah, M., Ebisuzaki, W., Higgins, W., Janowiak, J., Mo, K. C., Ropelewski, C., Wang, J., Leetmaa, A., Reynolds, R., Jenne, R., and Joseph, D.: The NCEP/NCAR 40-Year Reanalysis Project, Bulletin of the American Meteorological Society, 77, 437 – 472, https://doi.org/https://doi.org/10.1175/1520-0477(1996)077<0437:TNYRP>2.0.CO;2, 1996.

Kara, G. T. and Elbir, T.: Evaluation of ERA5 and MERRA-2 Reanalysis Datasets over the Aegean Region, Türkiye, Dokuz Eylül Üniversitesi Mühendislik Fakültesi Fen ve Mühendislik Dergisi, 26, 9–21.

Kathayat, G., Sinha, A., Tanoue, M., Yoshimura, K., Li, H., Zhang, H., and Cheng, H.: Interannual oxygen isotope variability in Indian summer monsoon precipitation reflects changes in moisture sources, Communications Earth & Environment, 2, 96, 2021.

Kesarwani, M., Neeti, N., and Chowdary, V.: Evaluation of different gridded precipitation products for drought monitoring: a case study of Central India, Theoretical and Applied Climatology, 151, 817–841, 2023.

Kulkarni, J., Maheskumar, R., Konwar, M., Deshpande, C., Morwal, S., Padma Kumari, B., Joshi, R., Pandithurai, G., Bhalwankar, R., Mujumdar, V., et al.: The Cloud Aerosol Interactions and Precipitation Enhancement Experiment (CAIPEEX): overview and prominent results, in: AGU Fall Meeting Abstracts, vol. 2009, pp. A13K–01, 2009.

Kumar, R., Naja, M., Pfister, G. G., Barth, M. C., and Brasseur, G. P.: Simulations over South Asia using the Weather Research and Forecasting model with Chemistry (WRF-Chem): set-up and meteorological evaluation, Geoscientific Model Development, 5, 321–343, https://doi.org/10.5194/gmd-5-321-2012, 2012.

Lacima, A., Petetin, H., Soret, A., Bowdalo, D., Jorba, O., Chen, Z., Méndez Turrubiates, R. F., Achebak, H., Ballester, J., and Pérez García-Pando, C.: Long-term evaluation of surface air pollution in CAMSRA and MERRA-2 global reanalyses over Europe (2003–2020), Geoscientific Model Development Discussions, 2022, 1–37, 2022.

Lombard, F., Bourdin, G., Pesant, S., Agostini, S., Baudena, A., Boissin, E., Cassar, N., Clampitt, M., Conan, P., Da Silva, O., et al.: Open science resources from the Tara Pacific expedition across coral reef and surface ocean ecosystems, Scientific data, 10, 324, 2023.

Mahto, S. S., Nayak, M. A., Lettenmaier, D. P., and Mishra, V.: Atmospheric rivers that make landfall in India are associated with flooding, Communications Earth & Environment, 4, 120, 2023.

Malasani, C. R., Swain, B., Patel, A., Pulipatti, Y., Anchan, N. L., Sharma, A., Vountas, M., Liu, P., and Gunthe, S. S.: Modeling of mercury deposition in India: evaluating emission inventories and anthropogenic impacts, Environmental Science: Processes amp; Impacts, https://doi.org/10.1039/d4em00324a, 2024.

McCarty, W., Coy, L., Gelaro, R., Huang, A., Merkova, D., Smith, E. B., Sienkiewicz, M., and Wargan, K.: MERRA-2 input observations: Summary and assessment, NASA Tech. Rep. NASA/TM-2016-104606, 46, 64, 2016.

Meng, L., Liu, J., Tarasick, D. W., and Li, Y.: Biases of Global Tropopause Altitude Products in Reanalyses and Implications for Estimates of Tropospheric Column Ozone, Atmosphere, 12, 417, https://doi.org/10.3390/atmos12040417, 2021.

Mojgan, G. M., Mehdi, M. M., and Reza, B. M.: The trend of changes in surface wind in the Indian Ocean, in the period from 1981 to 2015, using reanalysis data, NCEP/NCAR, Open Journal of Marine Science, 7, 445–457, 2017.

Moorthy, K. K., Satheesh, S., Babu, S. S., and Dutt, C.: Integrated campaign for aerosols, gases and radiation budget (ICARB): an overview, Journal of Earth System Science, 117, 243–262, 2008.

https://doi.org/10.5194/egusphere-2025-4229
Preprint. Discussion started: 2 December 2025

Mujumdar, M., Preethi, B., Sabin, T., Ashok, K., Saeed, S., Pai, D., and Krishnan, R.: The Asian summer monsoon response to the La Nina event of 2010, Meteorological Applications, 19, 216–225, 2012.

Nair, S., Srinivasan, G., and Nemani, R.: Evaluation of multi-satellite TRMM derived rainfall estimates over a western state of India, Journal of the Meteorological Society of Japan. Ser. II, 87, 927–939, 2009.

Olsen, E. T., Aumann, H., Broberg, S., Chen, L., Elliott, D., Fetzer, E., Fishbein, E., Friedman, S., Gaiser, S., Granger, S., et al.: AIRS/AMSU/HSB version 4.0 data release user guide, Jet Propulsion Laboratory, California Institute of Technology, Pasadena, CA, 2005.

Rai, D. and Raveh-Rubin, S.: Enhancement of Indian summer monsoon rainfall by cross-equatorial dry intrusions, NPJ climate and atmospheric science, 6, 43, 2023.

Rai, P. and Dimri, A. P.: Effect of changing tropical easterly jet, low level jet and quasi-biennial oscillation phases on Indian summer monsoon, Atmospheric Science Letters, 18, 52–59, https://doi.org/https://doi.org/10.1002/asl.723, 2017.

Rajan, D. and Desamsetti, S.: Prediction of Indian summer monsoon onset with high resolution model: a case study, SN Applied Sciences, 3, 1–14, 2021.

Reichler, T., Dameris, M., and Sausen, R.: Determining the tropopause height from gridded data, Geophysical research letters, 30, 2003.

Satheesh, S., Vinoj, V., and Krishnamoorthy, K.: Assessment of aerosol radiative impact over oceanic regions adjacent to Indian subcontinent using multisatellite analysis, Advances in Meteorology, 2010, 139 186, 2010.

Seinfeld, J. H., Bretherton, C., Carslaw, K. S., Coe, H., DeMott, P. J., Dunlea, E. J., Feingold, G., Ghan, S., Guenther, A. B., Kahn, R., et al.: Improving our fundamental understanding of the role of aerosol- cloud interactions in the climate system, Proceedings of the National Academy of Sciences, 113, 5781–5790, 2016.

Shahi, N. K. and Rai, S.: An increase in widespread extreme precipitation events during the northeast monsoon season over south peninsular India, Scientific Reports, 13, 22 757, 2023.

Sharma, M., Singh, R., and Kathuria, A.: Climate change and the Indian economy–a review, Current World Environment: An International Research Journal of Environmental Sciences, 17, 20, 2022.

Shukla, A. K. and Shukla, S.: Satellite Precipitation Estimates (SPEs) and Their Validation Using Ground-Based Measurments: A Case Study in Uttarakhand State, India, in: IGARSS 2020-2020 IEEE International Geoscience and Remote Sensing Symposium, pp. 5360–5363, IEEE, 2020.

Shukla, A. K., Ojha, C. S. P., Singh, R. P., Pal, L., and Fu, D.: Evaluation of TRMM precipitation dataset over Himalayan catchment: the upper Ganga basin, India, Water, 11, 613, 2019.

Sijikumar, S., Aneesh, S., and Rajeev, K.: Multi-year model simulations of mineral dust distribution and transport over the Indian subcontinent during summer monsoon seasons, Meteorology and Atmospheric Physics, 128, 453–464, 2016.

Swain, B., Vountas, M., Singh, A., Anchan, N. L., Deroubaix, A., Lelli, L., Ziegler, Y., Gunthe, S. S., Bösch, H., and Burrows, J. P.: Aerosols in the central Arctic cryosphere: satellite and model integrated insights during Arctic spring and summer, Atmospheric Chemistry and Physics, 24, 5671–5693, 2024.

Tanimoto, H., Oanh, N. T. K., Naja, M., Lung, C., Latif, M. T., Yu, L., Salam, A., Cambaliza, M. O., Hien, T. T., Hlaing, O. M. T., et al.: Atmospheric chemistry research in Monsoon Asia and Oceania: Current status and future prospects, APN Sci. Bull., 10, 126–31, 2020.

Walker, J. R.: Qualitative Comparison of IGRA and ESRL Radiosonde Archived Databases, Tech. rep., 2014.

Wang, Y., Leung, L. R., McGREGOR, J. L., Lee, D.-K., Wang, W.-C., Ding, Y., and Kimura, F.: Regional climate modeling: progress, challenges, and prospects, Journal of the Meteorological Society of Japan. Ser. II, 82, 1599–1628, 2004.

https://doi.org/10.5194/egusphere-2025-4229
Preprint. Discussion started: 2 December 2025

Wargan, K., Labow, G., Frith, S., Pawson, S., Livesey, N., and Partyka, G.: Evaluation of the Ozone Fields in NASA's MERRA-2 Reanalysis, Journal of Climate, 30, 2961–2988, 2017.

Weldeab, S., Rühlemann, C., Ding, Q., Khon, V., Schneider, B., and Gray, W. R.: Impact of Indian Ocean surface temperature gradient reversals on the Indian Summer Monsoon, Earth and Planetary Science Letters, 578, 117 327, 2022.

Wen, A., Wu, T., Wu, X., Zhu, X., Li, R., Ni, J., Hu, G., Qiao, Y., Zou, D., Chen, J., et al.: Evaluation of MERRA-2 land surface temperature dataset and its application in permafrost mapping over China, Atmospheric Research, 279, 106 373, 2022.

Willmott, C. J.: On the validation of models, Physical geography, 2, 184–194, 1981.

Xavier, P. K., John, V. O., Buehler, S., Ajayamohan, R., and Sijikumar, S.: Variability of Indian summer monsoon in a new upper tropospheric humidity data set, Geophysical research letters, 37, 2010.

YADAV, R. K., RUPA KUMAR, K., and RAJEEVAN, M.: Characteristic features of winter precipitation and its variability over northwest India, Journal of Earth System Science, 121, 611–623, https://doi.org/10.1007/s12040-012-0184-8, 2012.

Zhao, W. and Li, A.: A review on land surface processes modelling over complex terrain, Advances in Meteorology, 2015, 607 181, 2015.

Zhu, R., Sun, C., and Yan, Y.: Formation mechanism and development potential of wind energy resources on the Tibetan plateau, Renewable Energy, 227, 120 527, 2024.